Charge Localization and Trapping in Lead-Iodide Perovskites: Role of Polarons and Defects in Material Stability for Biomedical and Optoelectronic Applications

Dr. Giulia Rossi[1]*, Dr. Marco Bianchi[1]

[1]Department of Materials Science and Nanomedicine Engineering, University of Milan Hospital, Milan, Italy

Abstract

Surfaces and grain boundaries play a fundamental role in charge transport, localization and trapping in polycrystalline thin films of metal halide perovskites. Comprehension of the phenomena occurring at the surface is thus crucial to increase solar cells efficiency and, most importantly, temporal stability. We investigate charge localization and trapping at the surface of the prototypical $MAPbI_3$ perovskite through advanced electronic-structure calculations, considering different surface terminations. Both MAI- or PbI_2-terminated surfaces attain a clear spatial separation of hole and electron polarons, while a MAI-vacant surface induces charge localization at under-coordinated lead atoms. Notably, the MAI-terminated surface is as defect-tolerant as bulk $MAPbI_3$, while the PbI_2-terminated surface is sensitive to surface defects, which may either act as recombination centres or inhibit charge transfer at the surface. We thus suggest that perovskite growth in MAI-rich conditions should be beneficial to limit surface recombination, while the synthesis of $MAPbI_3$ in a PbI_2-rich environment should be accompanied by surface passivation strategies to counteract the negative impact of surface defects.

1. Introduction

Metal halide perovskites of general formula ABX_3 have generated an unprecedented excitation in the growing field of third-generation photovoltaics.[1-3] Since the pioneering studies of only ten years ago, the photo-conversion efficiency of devices based on metal halide perovskites have rocketed from 4%[4] to >25%[5], a growth rate unequalled by other perspective materials for solar cells that have been investigated during the same time span. The extraordinary results achieved by this novel class of materials may provide a viable solution to complement or even replace silicon-based solar cells in the near future. However, the fulfilment of a such a goal is related to an in-depth comprehension of the electronic and stability properties of metal halide perovskites, which have eluded both measurements and theory for a long time. In particular, one of the key features behind the success of metal halide perovskites is the slow recombination of photogenerated carriers measured for both the most common mechanisms: *i.e.* (i) band-to-band transitions (bimolecular recombination) and (ii) transitions mediated by defects (monomolecular recombination).[6-10] This peculiar property has for long puzzled the scientific community. Therefore, large efforts have been devoted to explain how these atypical materials could match the performance of high-purity inorganic crystalline semiconductors.[11, 12] Early attempts of explaining the slow bimolecular recombination measured for lead halide perovskites focussed on the possible role of the organic A-site cations in screening the photogenerated exciton[13, 14] or in favouring different nanoscale localizations of valence and conduction band-edge states.[15, 16] However, bimolecular recombination coefficients measured for fully inorganic perovskites were found to be close to those of related perovskites bearing organic cations,[17] thus ruling out these explanations. The slow monomolecular recombination measured for these materials was even more puzzling. In fact, the low-temperature techniques used to synthesize metal halide perovskites are likely to provide high concentration of intrinsic defects,[18-20] some of which, in turn, are predicted to play a role in charge trapping and recombination from density functional theory calculations.[21] Nonetheless, these materials appear to be defect-tolerant.[22-24] Recent time-resolved Kerr-effect spectroscopy measurements and first-principles calculations indicated that charge carriers in lead halide perovskites

occur as large polarons,[25, 26] These results have significantly contributed to the shed fresh light on the physical picture behind the exceptional opto-electronic properties of lead halide perovskites. Polaron formation was found to occur on the sub-picosecond timescale,[25, 26] and therefore not compatible with the rotation of the organic cations. Furthermore, advanced molecular dynamics simulations performed on $MAPbI_3$ (MA=methylammonium) have shown that hole and electron polarons are rapidly separated in different regions of the material, upon photoexcitation. This feature is found to decrease the recombination rate by at least one order of magnitude, if compared to that pertinent of band-to-band transitions.[26] The polaronic nature of the charge carriers enables also to explain the defect tolerance of $MAPbI_3$. In fact, Wiktor *et al.* have shown that recombination of hole and electron on an interstitial iodine is limited by the synergistic effects of a small kinetic barrier and of the screened interaction between the hole polaron and the negatively charged iodine defect.[27] Finally, very recent *ab initio* calculations have revealed further insights on the nature of polarons in lead halide perovskites, as they are found to depend on a delicate balance between thermally induced disorder, driven by the motion of A-site cations, and polaron stabilization within the BX_3 sublattice.[28] A detailed investigation of polaron hopping within the material pointed out a mechanism guided by the random reorientation of the A-site cations,[28] which allowed to explain the observed low mobility[29] and high diffusion length of charge carriers.[10, 30, 31]

Although the comprehension of the outstanding properties of lead halide perovskites has seen remarkable advancements, further improvements of devices based on these materials is indeed possible, since the current efficiencies are still noticeably smaller than that predicted by the Shockley-Queisser limit.[32] On this regard, while most studies have focussed on the electronic properties of bulk materials, channels for charge loss and instabilities in working devices could originate from phenomena occurring at the surface and interface.[33, 34] It is well known that the surface of solution-processed lead halide perovskite is prone to the formation of defects, which could be noxious for the opto-electronic properties of the devices.[35-38] In fact, surface trap density was found to be up two order of magnitude larger than that of the bulk material and the diffusion length of charge carriers noticeably shorter.[39] Time-resolved spectroscopy

measurements have shown that surface recombination is faster in single crystals than in polycrystalline films, an instance possibly justified by defect passivation operated by the excess of MA in the non-stoichiometric samples.[37] In contrast, *ab initio* calculations performed by Tong *et. al.* indicated MA to be responsible for charge recombination at the surface and suggested that decreasing its concentration on the surface would be beneficial for the system.[40] Similarly, density functional theory (DFT) calculations performed on different models of $MAPbI_3$ indicate that PbI_2-rich condition would favour flat surfaces without mid-gap states.[41, 42] A large number of studies have focussed on the role of passivating layers on top of the surface, as they could minimize surface recombination,[43-47] possibly also extending the stability of the device. Furthermore, the surface termination can also determine a different alignment of energy levels at the interface, depending on the charge transfer layers used in the device. For example, it has been found that the favourable alignment between MAI-covered surfaces and C_{60} promotes electron transfer across the $MAPbI_3/C_{60}$ interface.[48] However, when a hole-transport material such as spiro-MeO-TAD is considered, the shift of the band edges towards the vacuum level induced by surface MAI hinder the hole transfer process.[49] Overall, since the physics of charge carriers at the surface is not completely understood, the design of viable solutions to simultaneously limit charge recombination and enhance charge transfer across the interface is lacking a rationale. Furthermore, current studies do not account for the polaronic nature of charge carriers, which could play a key role not only in the bulk but also on surfaces.

In this work, we study the electronic properties of the (001) surface of tetragonal $MAPbI_3$ by employing hybrid DFT calculations. Our analysis shows that hole and electron polarons localize in different regions of the slabs on the pristine PbI_2-terminated (PbI_2) and MAI-terminated (MAI) (001) surfaces. The reduced spatial overlap of electrons and holes hinders their recombination on these surfaces. On the other hand, for systems with a partial MAI coverage, hole and electron polarons appear to be spatially closer, thus the probability of recombination is enhanced. Furthermore, we observe the formation of a small electron polaron on the partially MAI-covered surface associated with a surface reconstruction around an unsaturated Pb ion on the surface, indicating that charge-trapping

processes are further enhanced on this surface. These results suggest that rough surfaces with partial coverages severely affect the efficiency of perovskite-based devices by promoting both radiative and non-radiative recombination through localized surface states.

In order to investigate the sources of non-radiative recombination, we include in our study the analysis of the stability and the trapping activity of native defects at these surfaces. By comparing the formation energies of surface and bulk defects, we observe that only the MA vacancy (V_{MA}), which produces a shallow energy level, is favoured on the MAI surface. In contrast, vacancies of Pb (V_{Pb}) and I (V_I) and the I interstitial (I_I) are more stable on the PbI_2-terminated surface. In particular, V_{Pb} and I_I, which feature mid-gap transition energy, can promote monomolecular charge recombination. Furthermore, the study of I_I shows that hole trapping on this defect involves the crossing of an energy barrier for both terminations, in line with previous results achieved for the bulk material.[27] The different spatial localizations of holes and electrons on the surfaces, however, dramatically enhance the probability of hole trapping at the defect in PbI_2-terminated surface with respect to the MAI-terminated surface and bulk $MAPbI_3$. At variance, surface V_I, while not directly acting as a recombination centre, does not support the formation of a hole polaron within the PbI_2 layer bearing it. This might prevent the migration of hole polarons on the surface, an occurrence which would be detrimental for interfacial charge transfer.

Finally, the consequences of the present results are discussed in view of the ongoing efforts to limit interfacial charge recombination and enhance charge transfer. On one side, synthesis of $MAPbI_3$ in a MAI-rich environment may be a satisfactory strategy for limiting the formation of PbI_2-rich surfaces, responsible of the increased monomolecular recombination, without affecting the defects tolerance of perovskites polycrystalline films. On the other hand, this should be coupled to a judicious choice of the materials used as charge transport layers, in order to achieve an optimal alignment of energy levels.[49]

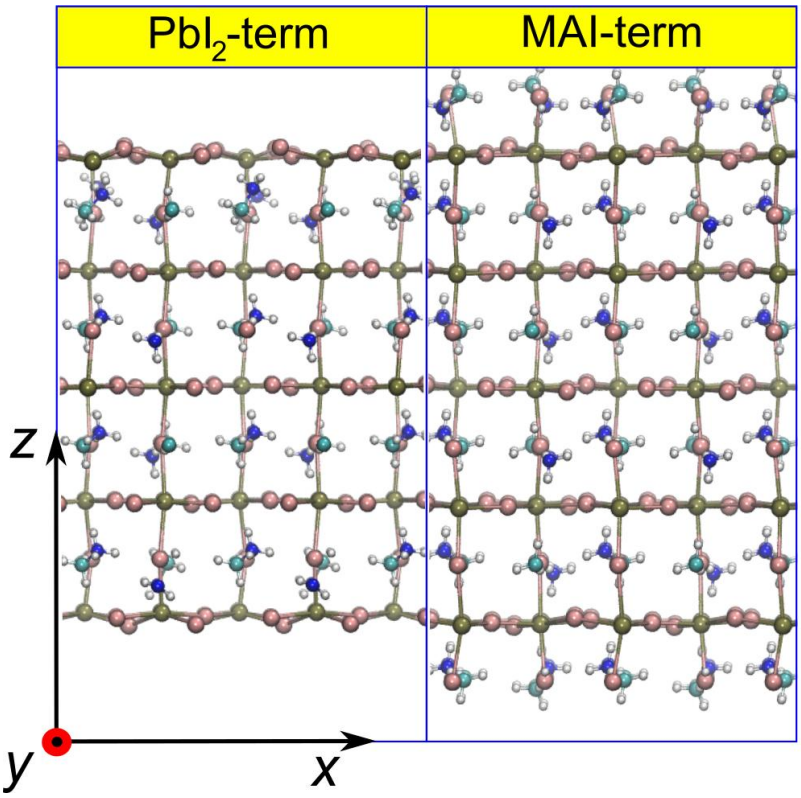

Figure 1. Stick&ball representation of the PbI_2 and MAI (001) surfaces of tetragonal $MAPbI_3$. Lead in brown, iodine in pink, nitrogen in blue, carbon in cyan, and hydrogen in white.

2. Methods

All DFT calculations are carried out at the hybrid-functional level with the PBE0 functional.[50, 51] The fraction of Fock exchange α is preserved to its original value (0.25), because it complies with the Koopmans' condition for this material,[52] thus ensuring that the calculations are essentially devoid of the self-interaction error,[26,53, 54] which would affect the energetics of the system and charge localization. We include non-local van der Waals interactions through the rVV10 scheme.[55, 56] Calculations are carried out with the freely-available CP2K suite of codes.[57] Goedecker-Teter-Hutter pseudopotentials are used to account for core-valence interactions.[58] We use double-ζ polarized basis sets for the wave functions[59] and a cut-off of 300 Ry for the expansion of the electron density in plane waves. We employ the auxiliary density matrix method to speed up the

calculation of exact exchange in hybrid functional calculations as implemented in CP2K with the cFIT auxiliary basis set.[60] We do not include spin-orbit coupling (SOC) in geometry optimizations, as this is not implemented in CP2K. While significantly contributing to the electronic properties of lead-halide perovskites [61, 62] the effect of SOC on valence band-edge states is rather limited.[63] This ensures that the properties of hole polarons, originated from the valence band, are properly captured by our computational approach. Furthermore, even if the position of the conduction band-edge states is noticeably influenced by SOC, [61, 62] previous studies have shown that the introduction of SOC have negligible effects on polaron localization[26] and on the calculated stabilization energies.[64] However, in one particular case (*vide infra*) additional calculations including SOC are carried out to properly describe an electron polaron, whose energetics is indeed sensitive to SOC. Calculations are performed on different models of the (001) surface of tetragonal $CH_3NH_3PbI_3$: (i) a 552-atoms slab terminated with methylammonium iodide (MAI), (cf. Fig. 1, left panel), (ii) a 408-atoms slab terminated with lead diiodide (PbI_2) (cf. Fig. 1, right panel) and (iii) slabs with partial MAI coverages. All the considered slabs possess the same thickness (5 PbI_2 layers) , the simulation cell has $a = b = 17.70$ Å, $c = 50$ Å, with the latter including a vacuum layer of 20 (25) Å for MAI (PbI_2) slab, a computational setup that has been benchmarked in previous studies.[49] In particular, we note that the position of the band edges is stable with respect to slab thickness. This implies that the energetics of defects, which is influenced by the position of band edges, is not affected by slab thickness.[49] Furthermore, in the Supplementary Information (SI), we verify that charge localization and the energetics of polarons are unaffected by the thickness of the slab, by performing extra calculations using slabs with 6 and 7 PbI_2 layers. We note that a previous study on polarons in the bulk material has shown that convergence of the charge density is achieved only when considering very large supercells (> 80 Å).[65] However, the effect of size on the energetics of polarons was found to be rather exiguous.[28] This ensures that the trends observed in this study are not affected by the employed supercell.

We focus on the (001) surface since both theoretical calculations[41, 66] and X-ray diffraction experiments[67] indicate that this one of the dominant facets in tetragonal $MAPbI_3$. Additional

calculations of defects performed for bulk tetragonal $MAPbI_3$ are carried out employing a 384-atoms 2×2×2 supercell with lattice parameters $a = b = 17.72$ Å, $c = 25.32$ Å.

To calculate the energy levels of polarons and defects in slabs of $MAPbI_3$, we adopt the grand-canonical formulation of defects in crystalline materials.[68, 69] This theory allows to express the formation energy of a defect X with charge q, $E_f^q[X]$ as a function of the electron chemical potential μ:

$$E_f^q[X] = E^q[X] - E[\mathrm{ref}] - \sum_i n_i\mu_i + q(\varepsilon_\mathrm{V} + \mu) + E_\mathrm{corr}^q \quad (1)$$

In Eq. 1, $E^q[X]$ is the total energy of the defect X in the charge state q, $E[\mathrm{ref}]$ the total energy of the pristine slab, μ_i is the chemical potential of the subtracted/added species i, ε_V the valence band edge of the pristine system, and E_corr^q is a correction term, here introduced to account for electrostatic finite-size effects of charged periodic supercells. The charge transition level $\mu(q/q')$ is defined as the electron chemical potential for which the formation energies of a defect X in the charge states q and q' are equal ($E_f^q[X] = E_f^{q'}[X]$):

$$\mu(q/q') = \frac{E^q[X] - E^{q'}[X]}{q' - q} + \frac{E_{corr}^q - E_{corr}^{q'}}{q' - q} - \varepsilon_\mathrm{V}. \quad (2)$$

To calculate the binding energies of hole and electron polarons, we consider the following reactions, respectively:

$$\mathrm{MAPbI_3} + h^+ \longrightarrow h_\mathrm{loc}, \quad (3)$$

$$\mathrm{MAPbI_3} + e^- \longrightarrow e_\mathrm{loc}, \quad (4)$$

From. Eqs. 3 and 4, the hole and electron polaron levels can then are defined as follows, respectively:

$$\mu(h_\mathrm{loc}) = E[h_\mathrm{loc}] - E[\mathrm{MAPbI_3}] + E_{corr}^{+1} - \varepsilon_\mathrm{V}, \quad (5)$$

$$\mu(e_{\mathrm{loc}}) = E[e_{\mathrm{loc}}] - E[\mathrm{MAPbI_3}] + E_{corr}^{-1} - \varepsilon_{\mathrm{V}}, \quad (6)$$

where $E[h_{\mathrm{loc}}]$ and $E[e_{\mathrm{loc}}]$ are the total energies of the hole and electron polarons, respectively, and $E[\mathrm{MAPbI_3}]$ the total energy of the pristine slab. Then, we define the polaron binding energies as $E_b(h^+) = \mu(h_{\mathrm{loc}})$ and $E_b(e^-) = \varepsilon_{\mathrm{C}} - \mu(e_{\mathrm{loc}})$ where ε_{C} is the conduction band edge of pristine slab.

Electrostatic finite size corrections for slabs are here taken into account, using the Freysoldt-Neugebauer-Van de Walle (FNV) scheme,[68, 70] as reformulated for surfaces and interfaces by Komsa and Pasquarello.[71] Within this scheme, we are able to separate (i) the spurious interactions between the periodically repeated charges and (ii) the interactions between physical image charges occurring because of the variation in the dielectric constant across the surface. In particular, we calculate the energy correction $E_{corr}^{q} = E_{iso} - E_{per} + q\Delta V$, where E_{per} is the electrostatic energy calculated for a model representing the employed supercell, E_{iso} the electrostatic energy obtained when uniformly scaling all the dimensions of thee supercell, and ΔV the shift in the electrostatic potential between the model and the DFT calculation. We calculate E_{corr}^{q} up to 0.35 eV for systems with $q = -2$.

Calculations of energy barriers for hole trapping on interstitial iodide are carried out using a modified version of the linear transit method[72] previously employed in Ref. 28. The coordinates of the two neighbouring polaronic structures R_i and R_j are linearly interpolated[72] according to the following expression: $R_\lambda = \lambda R_i + (1-\lambda)R_j$ where λ is the coupling parameter connecting the two models. The achieved structures are then allowed to undergo structural relaxation in which the organic cations are free to relax. In contrast, the positions of the atoms belonging to the inorganic sub-lattice are fixed. In this way, we avoid unstable and highly energetic structures due to linear interpolation of the coordinates of the freely-rotating organic cations.

Table 1. Calculated values of $E_b(h^+)$ and $E_b(e^-)$for different models of the (001) $MAPbI_3$ surface. All values are given in meV. In parenthesis, we indicate whether the polaron is in the bulk region (B) or on the surface (S) of the slab.

Surface	$E_b(h^+)$	$E_b(e^-)$
MAI	90 (B)	90 (S)
V_{MAI}	80 (B)	250 (S)
0.5 MAI	70 (S)	120 (S)
PbI_2	120 (S)	20 (B)

3. Results and discussion

For each system previously described, we perform structural relaxations in presence of an extra hole and an extra electron. In Table 1, we report the calculated values of $E_b(h^+)$ and $E_b(e^-)$. For the MAI surface, we observe hole polaron formation in an inner PbI_2 plane layer of the slab [cf. Fig. 2 (a)] The calculated $E_b(h^+)$ is 80 meV, essentially equivalent to that calculated for the bulk[26]. The localization is accompanied by contraction of Pb-I bonds in the plane, in accord with the anti-bonding nature of the valence band edge states. [26, 73] In particular the Pb–I bonds of the PbI_4 units undergo contractions up to 0.1 Å, with respect to the neutral system. At variance, a complete localization of the hole polaron on the surface is observed for the PbI_2 system, which is associated with a $E_b(h^+)$ of 120 meV [cf. Fig. 2 (c)], consistent with the larger distortions of under-coordinated surface atoms. In fact, not only the Pb–I bonds of the surface PbI_2 layer are subject to contraction similar to those observed for the MAI surface, but we observe also small (up to 0.05 Å) out-of-plane elongation of Pb-I bonds formed by surface Pb and bridging I atoms. Furthermore, the removal of MAI from the surface pushes the valence band towards lower energies (i.e. further from the vacuum level).[48, 49] Therefore, surface valence states due to unsaturated lead are found to be detached from the valence band maximum (VBM) and, therefore, favour hole localization. We

note, for instance, that for a 0.5 MAI covered surface, the hole is found to be partially localized on the surface [cf. Fig. 2 (b)], in line with this physical picture.

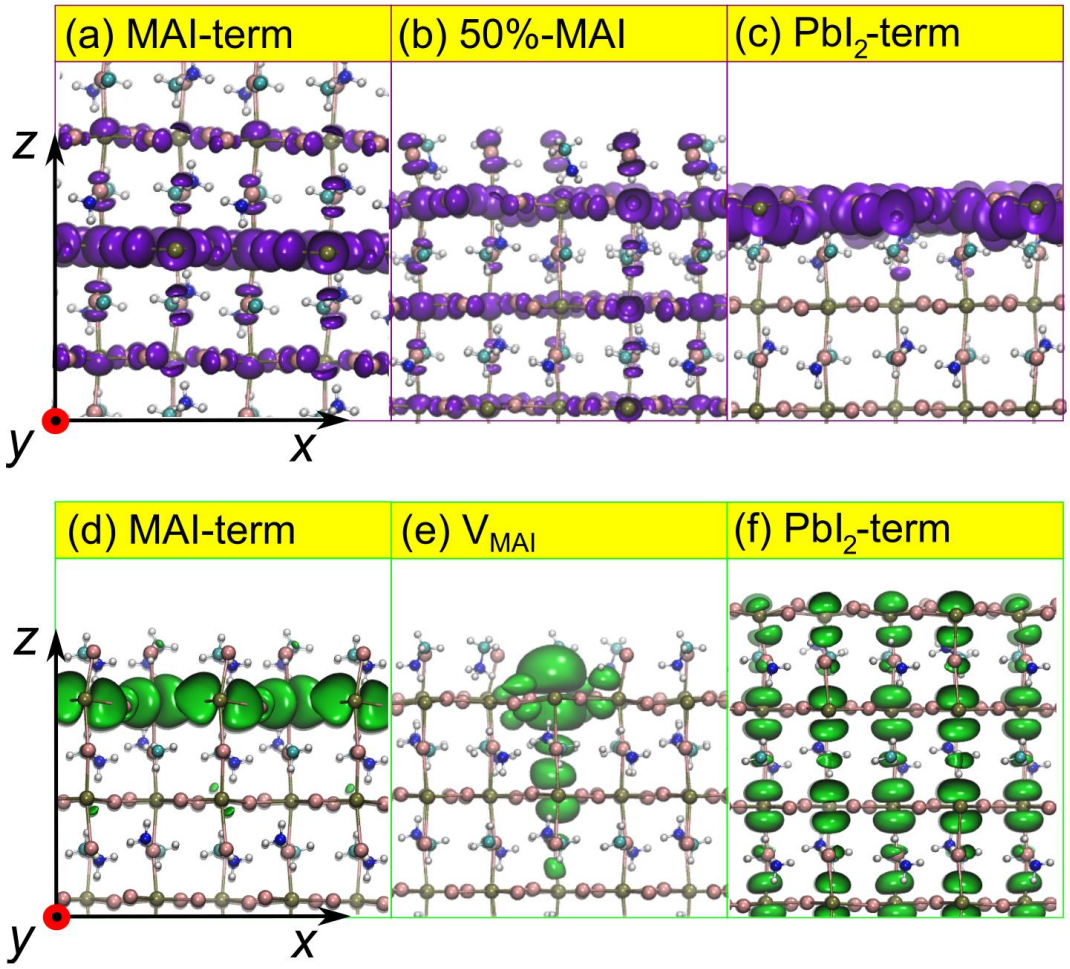

Figure 2. Isodensity representations of an extra hole (purple, upper panels) for (a) MAI surface, (b) 50% MAI-covered surface, and (c) PbI_2 surface. Isodensity representation of an extra electron (green, lower panels) for (d) MAI surface, (e) MAI-vacant surface (V_{MAI}), and (f) PbI_2 surface.

The electron polaron localizes on a sub-surface PbI_2 plane in the MAI slab [cf. Fig. 2 (d)], with $E_b(e^-) = 90$ meV, slightly larger than that observed for the corresponding polaron in the bulk (60 meV from Ref. 26). The localization is attained via an elongation of Pb-I bonds up to 0.15 Å, which is consistent with the weak anti-bonding hybridization between Pb 6p and I 5p in the conduction band. Furthermore, in analogy with the observations made for the hole polaron, MAI coverage moves the

conduction band closer to the vacuum level, [48, 49] which in turn causes the emergence of unoccupied surface states in the PbI_2 layer below the terminal MAI one. When the extra electron is introduced in the PbI_2 system, it appears to be semi-localized [cf. Fig. 2 (f)]. with a small $E_b(e^-)$ (20 meV). Also for the extra electron, we investigate the nature of polarons on surfaces with mixed coverages. In particular, upon removal of a single MAI unit from the surface (V_{MAI}), we observe the transition from a large to a small polaron. The negative charge is localized almost completely on an under-coordinated sub-surface Pb^{2+} [cf. Fig. 2 (e)] and a large $E_b(e^-)$ of 250 meV is calculated. Furthermore, a significant surface reconstruction is observed with the involved lead atom being shifted upwards by almost 0.4 Å, thus suggesting a possible degradation mechanism of the defective surface in electron-rich conditions. We notice that a similar localization is retained up to 0.5 MAI coverage of the surface. We further extend this analysis by introducing a second electron in the system bearing a surface MAI vacancy. The second electron is also localized on the unsaturated surface Pb [as in Fig. 2 (e)], which is significantly displaced from its equilibrium position in the neutral system. As the ejection of metallic lead clusters from $MAPbI_3$ is observed experimentally under electron-rich conditions,[74] these results indeed suggest that this degradation mechanism of $MAPbI_3$ can be related to electron trapping by under-coordinated Pb atoms.

Since SOC could be particularly relevant in this case, as we are adding electrons to Pb-based unoccupied states, we performed supplementary calculations with the QUANTUM ESPRESSO code[75] employing full relativistic pseudopotentials.[76] In particular, we compare the total energies of the slab featuring a single surface MAI vacancy (i) upon vertical injection of the electron E_v and (ii) after reconstruction E_r, i.e. the so-called stabilization energy: $E_s = E_v - E_r$. At the PBE[77]+SOC level of theory, $E_s = -0.40$ eV, hence the polaronic structure is found to be less stable. However, at the PBE0 level, $E_s = 0.55$ eV. Finally, when both exact exchange and relativistic effects are included at the PBE0+SOC level, $E_s = -0.1$ eV. We notice that this value is a lower limit because the calculations at 0 K do not include thermal effects, which are known to

favour the stabilization of polarons in $MAPbI_3$.[26, 28] Therefore, the proposed physical picture of electron localization on defective surface Pb atom is qualitatively retained when SOC is accounted for, although the stabilization energy is significantly reduced.

By comparing the results obtained for the different systems, we observe a distinct localization of holes and electrons for the pristine PbI_2 and MAI (001) surfaces, which can reduce the probability of interaction and thus recombination of photo-generated charges. Furthermore, the charge carriers appear both as large polarons, which are less sensitive to the detrimental charge-trapping processes.[78, 79] This result suggests that recombination of charge carriers should be reduced in these cases. In contrast, for rough surface with a partial MAI coverage, we observe two phenomena that could be noxious for a perovskite-based solar cells: (i) hole and electron appear to be both localized close to the surface and (ii) the electron localizes as a small polaron, which could promote charge trapping and hinder charge transport.[80, 81] Additionally, electron trapping at under-coordinated surface lead atoms may also promote material degradation by trapping of a second electron, which may act as a precursor in the release of lead atoms as metallic lead clusters observed in experiments.[74]

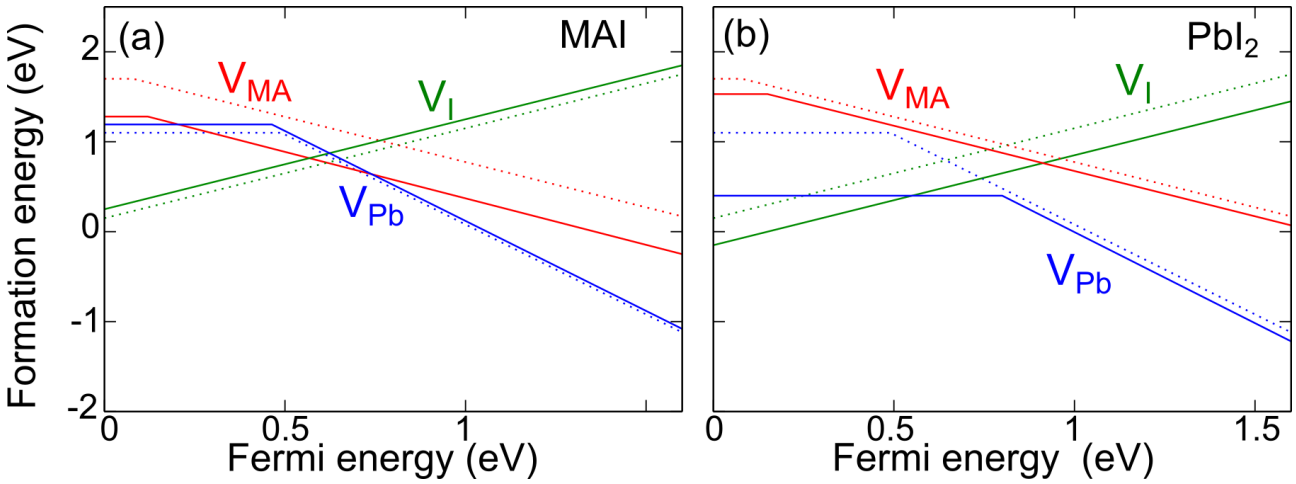

Figure 3. Formation energies of vacancies as a function of the electron chemical potential μ on the (a) MAI and (b) PbI_2 (001) terminated $MAPbI_3$ surface. Dashed lines for the respective values calculated for the bulk material. We consider iodine medium conditions as estimated in Ref. [82],

which correspond to $\mu_{MA} = -1.71$ eV , $\mu_{Pb} = -1.43$ eV, $\mu_I = -0.81$ eV. The conduction band edge is placed on the energy diagram by adding the experimental band gap[83] of $MAPbI_3$ to the valence band edge.

To provide a comprehensive picture of possible charge trapping occurring at surfaces, we consider the physics of point defects commonly encountered in $MAPbI_3$. First, we focus on the Pb, I, and MA vacancies (V_{Pb}, V_I and V_{MA} respectively) on both MAI and PbI_2 slabs. For each system, we compare the formation energies of the surface defects with those calculated for the bulk (cf. Fig. 3). For the MAI slab, the terminal PbI_2 plane is covered by MAI (cf. Fig. 1). In this system V_{MA} and V_I have been thus modelled by removing MA and I from the surface MAI layer, while V_{Pb} is created within the PbI_2 layer below it. The analysis of the calculated formation energies highlights that V_I and V_{Pb} are slightly less stable (~0.1 eV for the neutral defect and < 0.1 eV for the -1 charge state) than the corresponding defects in the bulk defects (cf. Fig. 3). In contrast, the surface V_{MA} is remarkably more stable (~0.5 eV for both 0 and -1 charge states) than the relative bulk defect. The calculated charge transition levels of these defects retain many features of the same defects in the bulk. In particular, we observe only shallow charge transition levels for V_I and V_{MA}, which are stable in the positive and negative states of charge, respectively, throughout almost the entire band gap of the material. Therefore, these surface defects should not contribute to monomolecular recombination of charge carriers. On the other hand, energy levels in the band gap are observed for V_{Pb}, which are almost equivalent to those calculated for the bulk material.[82] When considering the PbI_2 slab (cf. Fig.3), we note that surface V_{Pb} and V_I are noticeably more stable than the corresponding bulk defects, in stark contrast with the trends observed for the MAI surface. For V_{Pb}, the calculated $\mu(0/-2)$ lies at mid-gap, 0.80 eV above the valence band edge, 0.3 eV above the value achieved for the bulk. A similar trend is observed also for $\mu(0/-1)$ and $\mu(-1/-2)$ (cf. Fig. 7). Hence, the surface Pb vacancy may act as recombination centre at the PbI_2 surface of $MAPbI_3$. We

note that, differently from previous works,[84, 85] the charge transition levels of V_{Pb} are found to deeper in the gap of $MAPbI_3$. This is due to the fact that we here use we employ hybrid functional calculations to better describe the electronic properties of $MAPbI_3$. Furthermore, we have here identified the iodide trimer (I_3^-) as the most stable structural configuration for V_{Pb}^0 [cf. Fig. 4 (c)], in line with previous observations for the bulk material. [63]. This configuration is 0.8 eV more stable than the one obtained by simply removing two electrons from surface V_{Pb}^{2-}, thus explaining the lower formation energy of V_{Pb}^0 and the deeper energy levels.

Structural analysis of the surface defect reveals that for the negative V_{Pb}^{2-}, Pb-I bonds involving under-coordinated I atoms around the vacancy are found to be noticeably shrunk by 0.2 Å [cf. Fig 4 (a)]. When an extra hole is added to the system bearing V_{Pb}^{2-}, a hole polaron is localized in the PbI_2 plane bearing the vacancy [cf. Fig. 4 (b)]. Finally, upon injection of a second hole in the system, we observe the formation of an iodide trimer accompanying the localization of the charge and the oxidation of one iodine. This is achieved upon migration of surface I atom towards the vacancy [cf. Fig. 4 (c)]. The increased stability of the surface V_{Pb}^0 on the PbI_2 surface, which is mainly responsible for the deeper charge transition levels is due to both electronic and structural effects: in fact, the localization of two holes on a surface defect is energetically more favourable since holes are found to be drawn towards the PbI_2 surface. Furthermore, the structural analysis reveals that the surface triiodide formed in V_{Pb}^0 is less distorted than the bulk one, thus motivating the observed difference in formation energies [cf. SI for a detailed comparison of the local structures of bulk and surface V_{Pb}^0].

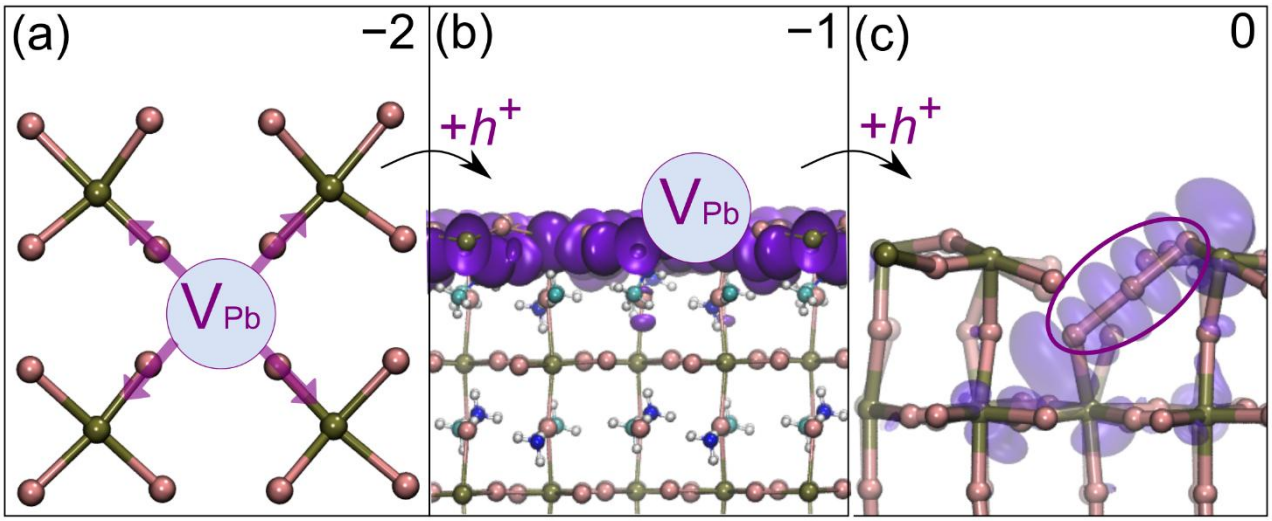

Figure 4. (a) Top view of the surface reconstruction on the PbI_2 plane of the (001) surface of tetragonal $MAPIbI_3$ for V_{Pb} in the −2 charge state. We only show one plane of Pb and I atoms for clarity. (b) Isodensity representation (side view) of an extra hole introduced in the system (see main text). Red, orange, and yellow isodensities correspond to systems bearing V_{Pb} in different positions, as illustrated in the figure. (c) Isodensity representation (side view) of hole trapping on surface V_{Pb}^{0}. The trimer formed upon displacement of a surface I atom (cf. main text) is circled and, for clarity, MA molecules are not shown.

At variance with this, V_I does not feature mid-gap states and apparently does to not represent an issue for recombination at the surface. However, structural and electronic analysis reveal a mechanism that could possibly affect charge transfer at the surface. In fact, in surface V_I^+, the under-coordinated Pb atoms are found to move far from the vacancy, while two I atoms get closer to each other by ~0.3 Å. As a consequence, the associated Pb-I bonds are elongated [cf. Fig.5 (a)]. Analysis of the VBM of the system in the +1 charge state shows that the observed bond elongation and the presence of the positively charged defect prevent the formation of the surface hole polaron in the plane featuring V_I^+. For instance, the surface hole polaron, observed for the pristine PbI_2 slab (cf. Fig. 2), is not found on the terminal PbI_2 plane featuring V_I but on a sub-surface plane [cf. Fig. 5 (b)]. Therefore, the Pb-I bonds elongations associated with V_I destabilize hole polarons

suggesting that, while not acting as a recombination centre, surface V_I may slow down or even inhibit the migration of the hole polaron to the surface, possibly affecting interfacial charge transfer.

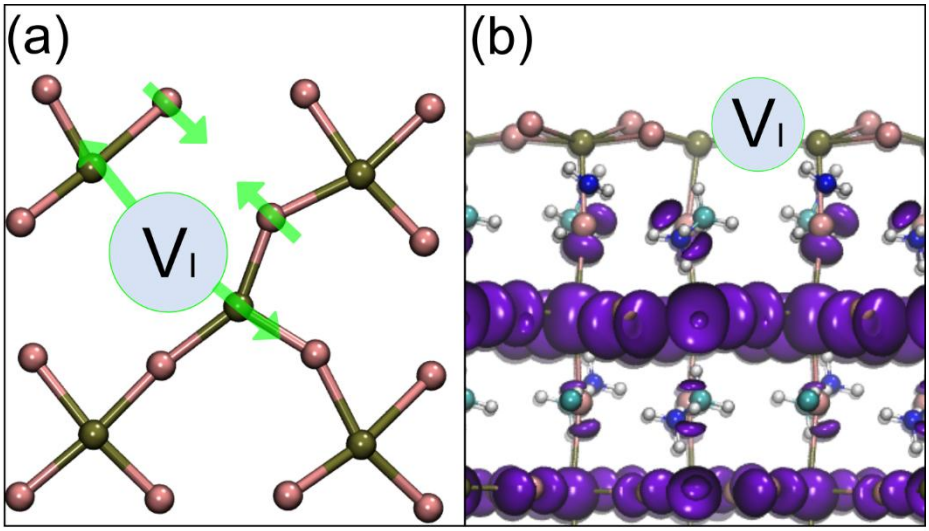

Figure 5. (a) Top view of the surface reconstruction on the PbI_2 plane of the (001) surface of tetragonal $MAPIbI_3$ for V_I in the +1 charge state. We only show one plane of Pb and I atoms for clarity. (b) Isodensity representation of the VBM for the PbI_2 surface (side view) bearing a V_I in the −1 charge state. The position of the vacancy is highlighted in the figure.

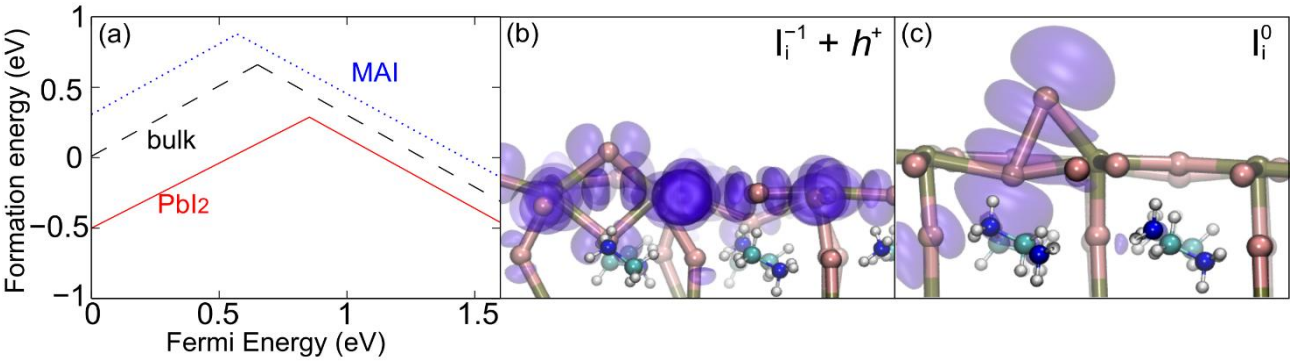

Figure 6. (a) Formation energies of I_i as a function of the electron chemical potential μ on the MAI (blue dotted) and PbI_2 (red solid) (001) $MAPbI_3$ surfaces. Black dashed line for the respective values calculated for the bulk material. We consider iodine medium conditions as estimated in Ref.

[82], which correspond to $\mu_{MA} = -1.71$ eV , $\mu_{Pb} = -1.43$ eV, $\mu_I = -0.81$ eV. The conduction band edge is placed on the energy diagram by adding the experimental band gap[83] of $MAPbI_3$ to the valence band edge. Side view of the PbI_2-terminated (001) surface of $MAPbI_3$ containing (b) the negatively charged interstitial I_i^{-1} and a hole polaron (left panel) and (c) the neutral I forming the I_2 dimer (centre panel). Isodensity representation of the hole is given in shaded purple.

We next investigate the energetics of the surface iodine interstitial I_i, which may appear in three different charged states: $+1$, 0, and -1. For the MAI surface, we observe that I_i^+ is remarkably less stable than in the bulk, as the formation energy of the defect is found to be 0.25 eV higher [cf. Fig. 6 (a)]. A similar trend is observed also for the neutral defect (not shown). This is consistent with the previously observed tendency of hole polarons to not localize on this surface termination. The energy difference is slightly reduced when considering the -1 state, but the bulk defect is still favoured. In contrast, surface I_i is more stable on the PbI_2 termination, particularly for the charge states envisaging localization of positive charge on the surface (0 and $+1$), in accord with its capability of attracting hole polarons. As a consequence, the charge transition level $\mu(+1/-1)$ is shifted towards lower (higher) energy values for the MAI (PbI_2) surfaces (cf. Fig. 6 (a)]. We note that a previous study on the bulk I_i has proved that recombination of holes and electrons is prevented by the combined effects of (i) a kinetic barrier for hole trapping on the defect and (ii) a reduced interaction between the positive charge and the negatively charged iodine defect, the latter being mainly induced by the fast hopping of the hole polaron within the material.[27] We here observe that, upon injection of a hole in the surface I_i^-, the injected positive charge localizes as a bulk-like and surface hole polaron for the MAI and PbI_2 surfaces, respectively [cf. Fig. 6(b) for the PbI_2 surface]. Therefore, the formation of the I_2 dimer, associated with the I_i^0 defect [cf. Fig. 6(b) for the PbI_2 surface] implies the overcoming of an energy barrier also for the surface defect. We here employ a modified linear transit method[72] (cf. Section 2) and we estimate energy barriers for the reaction $I_I^- + h^+ \rightarrow I_I^0$ of 0.10 and 0.20 eV for the PbI_2 and MAI surface, respectively. While the calculated

barriers are small if compared to intrinsic errors in DFT calculations, we note that the calculated formation energies of surface I_i indicate that such defect is present in lower densities on the MAI surface than in the bulk $MAPbI_3$. Furthermore, the hole trapping on the defect at the surface is prevented not only but the presence of an energy barrier but also by the preferential localization in the bulk-like region of the slab for this surface termination. For these reasons, we expect that this defect plays only a marginal role in the surface recombination processes. At variance with this, surface I_i is more stable than the bulk defect on the PbI_2 surface and the pinning of the hole polaron on the terminal PbI_2 layer increases the probability of interaction with the negatively charged defect and consequently that of overcoming the small energy barrier, thus ultimately enhancing the monomolecular recombination.

Overall, the present results allow to rationalize some of the practices adopted to limit the recombination of charge carriers at the interface and reconcile contrasting results previously reported. In Fig. 6, we report the relevant energy levels calculated for surface polarons and surface defects on the (001) MAI and PbI_2 slabs of tetragonal $MAPbI_3$. First of all, surface termination determines a preferential localization of hole and electron polarons, with the former localizing on the PbI_2 surface and the latter on the MAI one. Analysis of a system with half MAI coverage suggests that rough surfaces would open recombination channels within the material, due to the increased interaction between charge carriers, and could imply a possible degradation mechanism of the surface. The analysis of surface defects for the MAI system indicate that the only defect which is stabilized with respect to the bulk is V_{MA} (cf. Fig. 3), which however still gives a shallow charge transition level (cf. Fig. 6). The substantial preservation of the defect tolerance typical of the bulk material for the MAI surface model is in agreement with measurements that relate the reduced charge recombination in polycrystalline samples with excess MA cations passivating the surface. [37] In contrast, the results achieved for the PbI_2 model evidences that the unsaturated Pb and I surface atoms are subject to substantial displacements. This, in turn, stabilize the surface defects and brings either to the formation of surface recombination centres (V_{Pb}, I_i) or to defects disadvantaging charge

localization at the surface (i.e. $V_{I,}$ cf. Fig. 4). The simultaneous high stabilities of surface V_{Pb} and I_i and the preferential localization of hole polarons on the PbI_2 surface make these defects possible monomolecular recombination centres. Therefore, while our results on the polaron localization confirm that the pristine PbI_2 surfaces would not favour recombination since we observe charge localization similar to that attained in the bulk, [40, 41] the enhanced trapping properties of V_{Pb} and I_i observed for this termination suggests that MAI-rich conditions should be preferred to reduce their activity at the surface. Finally, we note that the two different terminations possess largely different work functions (cf. Fig. 6 and Ref. 49) and, therefore, the alignment between $MAPbI_3$ and the charge transfer layers within the actual photovoltaic device should be taken into account for the design of novel architectures.

In summary, our results evidenced that the separate localization of charge carriers for pristine and flat surface MAI and PbI_2 terminations is perturbed when considering mixed and rough surfaces that experimentally showed higher recombination. The study of surface defects showed that MAI surfaces are as defect tolerant as the bulk system, thus suggesting that MAI rich conditions of growth are preferable to reduce monomolecular recombination at the surface. At variance, the PbI_2 surface needs to be passivated as features defects that could enhance recombination or limit interfacial charge transfer. We hope these results will serve as a guideline to further optimize the performance and temporal stability of lead-halide perovskites for optoelectronic applications.

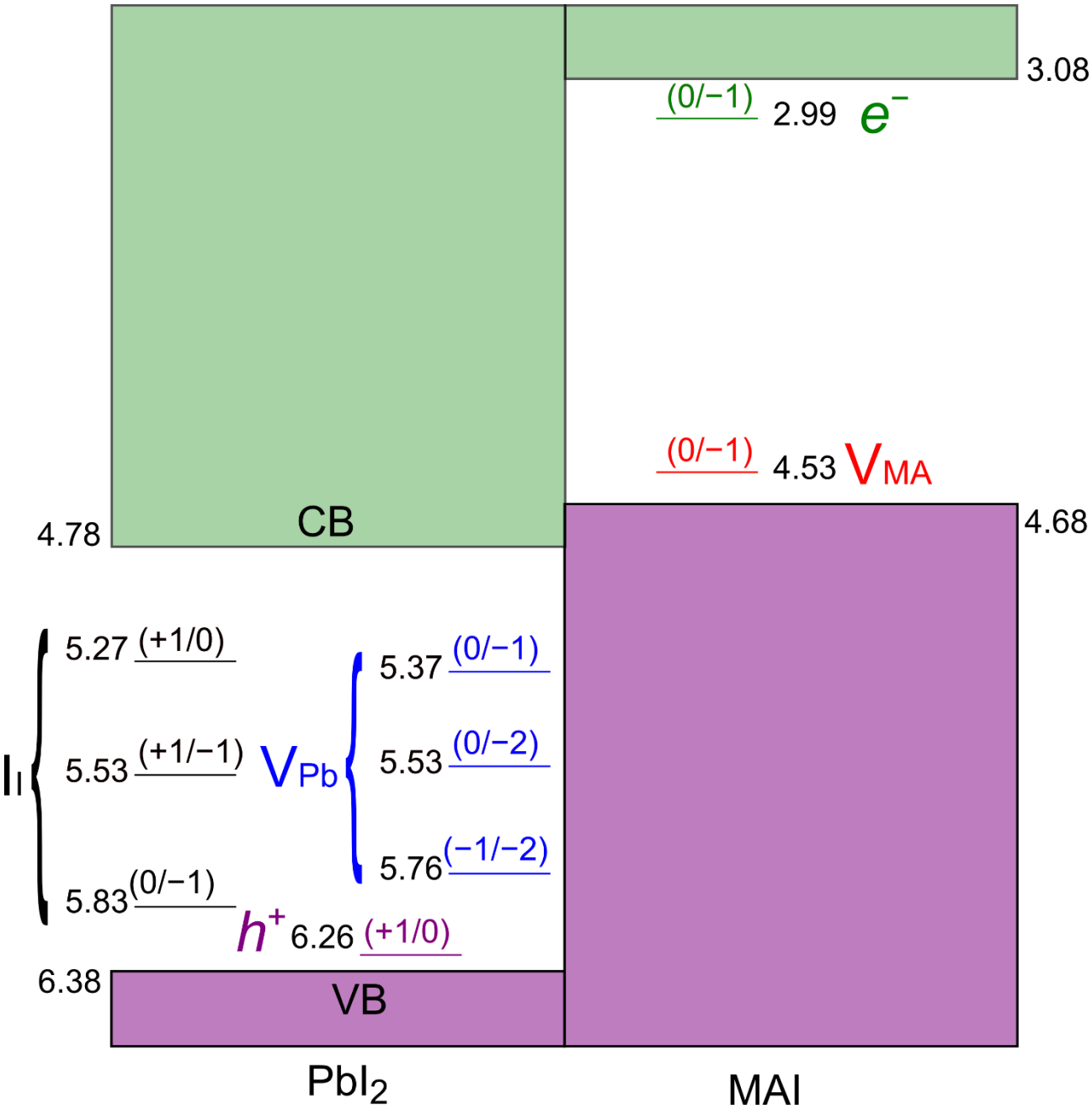

Figure 7. Schematic representation of the energy levels of surface defects which are relevant for the MAI and PbI_2 terminations of the (001) surface of tetragonal $MAPbI_3$. All energy levels are referred to the vacuum level, considering the work functions calculated in Ref. 49. The conduction band edge is placed on the energy diagram by adding the experimental band gap[83] of $MAPbI_3$ to the valence band edge.

Acknowledgment:

This project has received funding from the European Union's Horizon 2020 research and innovation programme under grant agreement No 764047 of the ESPRESSO project. The Ministero dell'Istruzione dell'Università e della Ricerca (MIUR) and Università degli Studi di Perugia are acknowledged for financial support through the program "Dipartimenti di Eccellenza 2018-2022" (Grant AMIS) to F.D.A.

References

1. Etgar, L.; Gao, P.; Xue, Z.; Peng, Q.; Chandiran, A. K.; Liu, B.; Nazeeruddin, M. K.; Grätzel, M., Mesoscopic CH3NH3PbI3/TiO2 Heterojunction Solar Cells. *Journal of the American Chemical Society* **2012,** *134* (42), 17396-17399.
2. Burschka, J.; Pellet, N.; Moon, S.-J.; Humphry-Baker, R.; Gao, P.; Nazeeruddin, M. K.; Grätzel, M., Sequential deposition as a route to high-performance perovskite-sensitized solar cells. *Nature* **2013,** *499*, 316.
3. Brenner, T. M.; Egger, D. A.; Kronik, L.; Hodes, G.; Cahen, D., Hybrid organic—inorganic perovskites: low-cost semiconductors with intriguing charge-transport properties. *Nature Reviews Materials* **2016,** *1*, 15007.
4. Kojima, A.; Teshima, K.; Shirai, Y.; Miyasaka, T., Organometal Halide Perovskites as Visible-Light Sensitizers for Photovoltaic Cells. *Journal of the American Chemical Society* **2009,** *131* (17), 6050-6051.
5. https://www.nrel.gov/pv/assets/images/efficiency-chart.png (accessed on 13 September 2019).
6. Ponseca, C. S.; Savenije, T. J.; Abdellah, M.; Zheng, K.; Yartsev, A.; Pascher, T.; Harlang, T.; Chabera, P.; Pullerits, T.; Stepanov, A.; Wolf, J.-P.; Sundström, V., Organometal Halide Perovskite Solar Cell Materials Rationalized: Ultrafast Charge Generation, High and Microsecond-Long Balanced Mobilities, and Slow Recombination. *Journal of the American Chemical Society* **2014,** *136* (14), 5189-5192.
7. Edri, E., E. Edri, S. Kirmayer, S. Mukhopadhyay, K. Gartsman, G. Hodes, and D. Cahen, Elucidating the charge carrier separation and working mechanism of CH3NH3PbI3− xClx perovskite solar cells, Nat. Commun. 5, 3461 (2014). *Nat. Commun.* **2014,** *5*, 3461.
8. Hutter, E. M.; Gélvez-Rueda, M. C.; Osherov, A.; Bulović, V.; Grozema, F. C.; Stranks, S. D.; Savenije, T. J., Direct–indirect character of the bandgap in methylammonium lead iodide perovskite. *Nature Materials* **2016,** *16*, 115.
9. Crothers, T. W.; Milot, R. L.; Patel, J. B.; Parrott, E. S.; Schlipf, J.; Müller-Buschbaum, P.; Johnston, M. B.; Herz, L. M., Photon Reabsorption Masks Intrinsic Bimolecular Charge-Carrier Recombination in CH3NH3PbI3 Perovskite. *Nano Letters* **2017,** *17* (9), 5782-5789.
10. Stranks, S. D.; Eperon, G. E.; Grancini, G.; Menelaou, C.; Alcocer, M. J. P.; Leijtens, T.; Herz, L. M.; Petrozza, A.; Snaith, H. J., Electron-Hole Diffusion Lengths Exceeding 1 Micrometer in an Organometal Trihalide Perovskite Absorber. *Science* **2013,** *342* (6156), 341-344.
11. Filippetti, A.; Delugas, P.; Mattoni, A., Radiative Recombination and Photoconversion of Methylammonium Lead Iodide Perovskite by First Principles: Properties of an Inorganic Semiconductor within a Hybrid Body. *The Journal of Physical Chemistry C* **2014,** *118* (43), 24843-24853.
12. Sell, D. D.; Casey, H. C., Optical absorption and photoluminescence studies of thin GaAs layers in GaAs–AlxGa1−xAs double heterostructures. *Journal of Applied Physics* **1974,** *45* (2), 800-807.

13. Frost, J. M.; Butler, K. T.; Brivio, F.; Hendon, C. H.; van Schilfgaarde, M.; Walsh, A., Atomistic Origins of High-Performance in Hybrid Halide Perovskite Solar Cells. *Nano Letters* **2014,** *14* (5), 2584-2590.
14. Even, J.; Pedesseau, L.; Katan, C., Analysis of multivalley and multibandgap absorption and enhancement of free carriers related to exciton screening in hybrid perovskites. *The Journal of Physical Chemistry C* **2014,** *118* (22), 11566-11572.
15. Ma, J.; Wang, L.-W., Nanoscale Charge Localization Induced by Random Orientations of Organic Molecules in Hybrid Perovskite CH3NH3PbI3. *Nano Letters* **2015,** *15* (1), 248-253.
16. Quarti, C.; Mosconi, E.; De Angelis, F., Structural and electronic properties of organo-halide hybrid perovskites from ab initio molecular dynamics. *Physical Chemistry Chemical Physics* **2015,** *17* (14), 9394-9409.
17. Dastidar, S.; Li, S.; Smolin, S. Y.; Baxter, J. B.; Fafarman, A. T., Slow Electron–Hole Recombination in Lead Iodide Perovskites Does Not Require a Molecular Dipole. *ACS Energy Letters* **2017,** *2* (10), 2239-2244.
18. Xing, G.; Mathews, N.; Sun, S.; Lim, S. S.; Lam, Y. M.; Grätzel, M.; Mhaisalkar, S.; Sum, T. C., Long-Range Balanced Electron- and Hole-Transport Lengths in Organic-Inorganic CH₃NH₃PbI₃. *Science* **2013,** *342* (6156), 344.
19. Ball, J. M.; Lee, M. M.; Hey, A.; Snaith, H. J., Low-temperature processed meso-superstructured to thin-film perovskite solar cells. *Energy & Environmental Science* **2013,** *6* (6), 1739-1743.
20. You, J.; Hong, Z.; Yang, Y.; Chen, Q.; Cai, M.; Song, T.-B.; Chen, C.-C.; Lu, S.; Liu, Y.; Zhou, H., Low-Temperature Solution-Processed Perovskite Solar Cells with High Efficiency and Flexibility. *ACS Nano* **2014,** *8* (2), 1674-1680.
21. Du, M.-H., Density Functional Calculations of Native Defects in CH3NH3PbI3: Effects of Spin–Orbit Coupling and Self-Interaction Error. *The Journal of Physical Chemistry Letters* **2015,** *6* (8), 1461-1466.
22. Kim, J.; Lee, S.-H.; Lee, J. H.; Hong, K.-H., The Role of Intrinsic Defects in Methylammonium Lead Iodide Perovskite. *The Journal of Physical Chemistry Letters* **2014,** *5* (8), 1312-1317.
23. Yamada, Y.; Endo, M.; Wakamiya, A.; Kanemitsu, Y., Spontaneous Defect Annihilation in CH3NH3PbI3 Thin Films at Room Temperature Revealed by Time-Resolved Photoluminescence Spectroscopy. *The Journal of Physical Chemistry Letters* **2015,** *6* (3), 482-486.
24. Buin, A.; Pietsch, P.; Xu, J.; Voznyy, O.; Ip, A. H.; Comin, R.; Sargent, E. H., Materials Processing Routes to Trap-Free Halide Perovskites. *Nano Letters* **2014,** *14* (11), 6281-6286.
25. Miyata, K.; Meggiolaro, D.; Trinh, M. T.; Joshi, P. P.; Mosconi, E.; Jones, S. C.; De Angelis, F.; Zhu, X.-Y., Large polarons in lead halide perovskites. *Science Advances* **2017,** *3* (8), e1701217.
26. Ambrosio, F.; Wiktor, J.; De Angelis, F.; Pasquarello, A., Origin of low electron–hole recombination rate in metal halide perovskites. *Energy & Environmental Science* **2018,** *11* (1), 101-105.
27. Wiktor, J.; Ambrosio, F.; Pasquarello, A., Mechanism suppressing charge recombination at iodine defects in CH3NH3PbI3 by polaron formation. *Journal of Materials Chemistry A* **2018,** *6* (35), 16863-16867.
28. Ambrosio, F.; Meggiolaro, D.; Mosconi, E.; De Angelis, F., Charge Localization, Stabilization, and Hopping in Lead Halide Perovskites: Competition between Polaron Stabilization and Cation Disorder. *ACS Energy Letters* **2019,** *4* (8), 2013-2020.
29. Brenner, T. M.; Egger, D. A.; Rappe, A. M.; Kronik, L.; Hodes, G.; Cahen, D., Are Mobilities in Hybrid Organic–Inorganic Halide Perovskites Actually "High"? *The Journal of Physical Chemistry Letters* **2015,** *6* (23), 4754-4757.
30. Kubicki, D. J.; Prochowicz, D.; Hofstetter, A.; Péchy, P.; Zakeeruddin, S. M.; Grätzel, M.; Emsley, L., Cation Dynamics in Mixed-Cation (MA)x(FA)1–xPbI3 Hybrid Perovskites from Solid-State NMR. *Journal of the American Chemical Society* **2017,** *139* (29), 10055-10061.
31. Gong, J.; Yang, M.; Ma, X.; Schaller, R. D.; Liu, G.; Kong, L.; Yang, Y.; Beard, M. C.; Lesslie, M.; Dai, Y.; Huang, B.; Zhu, K.; Xu, T., Electron–Rotor Interaction in Organic–Inorganic Lead Iodide Perovskites Discovered by Isotope Effects. *The Journal of Physical Chemistry Letters* **2016,** *7* (15), 2879-2887.
32. Rühle, S., Tabulated values of the Shockley–Queisser limit for single junction solar cells. *Solar Energy* **2016,** *130*, 139-147.
33. Schulz, P.; Cahen, D.; Kahn, A., Halide Perovskites: Is It All about the Interfaces? *Chemical Reviews* **2019,** *119* (5), 3349-3417.

34. Ono, L. K.; Qi, Y., Surface and Interface Aspects of Organometal Halide Perovskite Materials and Solar Cells. *The Journal of Physical Chemistry Letters* **2016,** *7* (22), 4764-4794.
35. Shi, D.; Adinolfi, V.; Comin, R.; Yuan, M.; Alarousu, E.; Buin, A.; Chen, Y.; Hoogland, S.; Rothenberger, A.; Katsiev, K.; Losovyj, Y.; Zhang, X.; Dowben, P. A.; Mohammed, O. F.; Sargent, E. H.; Bakr, O. M., Low trap-state density and long carrier diffusion in organolead trihalide perovskite single crystals. *Science* **2015,** *347* (6221), 519.
36. Bai, Y.; Meng, X.; Yang, S., Interface Engineering for Highly Efficient and Stable Planar p-i-n Perovskite Solar Cells. *Advanced Energy Materials* **2018,** *8* (5), 1701883.
37. Yang, Y.; Yang, M.; Moore, David T.; Yan, Y.; Miller, Elisa M.; Zhu, K.; Beard, Matthew C., Top and bottom surfaces limit carrier lifetime in lead iodide perovskite films. *Nature Energy* **2017,** *2*, 16207.
38. Sherkar, T. S.; Momblona, C.; Gil-Escrig, L.; Ávila, J.; Sessolo, M.; Bolink, H. J.; Koster, L. J. A., Recombination in Perovskite Solar Cells: Significance of Grain Boundaries, Interface Traps, and Defect Ions. *ACS Energy Letters* **2017,** *2* (5), 1214-1222.
39. Wu, B.; Nguyen, H. T.; Ku, Z.; Han, G.; Giovanni, D.; Mathews, N.; Fan, H. J.; Sum, T. C., Discerning the Surface and Bulk Recombination Kinetics of Organic–Inorganic Halide Perovskite Single Crystals. *Advanced Energy Materials* **2016,** *6* (14), 1600551.
40. Tong, C.-J.; Li, L.; Liu, L.-M.; Prezhdo, O. V., Long Carrier Lifetimes in PbI2-Rich Perovskites Rationalized by Ab Initio Nonadiabatic Molecular Dynamics. *ACS Energy Letters* **2018,** *3* (8), 1868-1874.
41. Haruyama, J.; Sodeyama, K.; Han, L.; Tateyama, Y., Termination Dependence of Tetragonal CH3NH3PbI3 Surfaces for Perovskite Solar Cells. *The Journal of Physical Chemistry Letters* **2014,** *5* (16), 2903-2909.
42. Uratani, H.; Yamashita, K., Charge Carrier Trapping at Surface Defects of Perovskite Solar Cell Absorbers: A First-Principles Study. *The Journal of Physical Chemistry Letters* **2017,** *8* (4), 742-746.
43. Xu, J.; Buin, A.; Ip, A. H.; Li, W.; Voznyy, O.; Comin, R.; Yuan, M.; Jeon, S.; Ning, Z.; McDowell, J. J.; Kanjanaboos, P.; Sun, J.-P.; Lan, X.; Quan, L. N.; Kim, D. H.; Hill, I. G.; Maksymovych, P.; Sargent, E. H., Perovskite–fullerene hybrid materials suppress hysteresis in planar diodes. *Nature Communications* **2015,** *6*, 7081.
44. Zhang, H.; Wu, Y.; Shen, C.; Li, E.; Yan, C.; Zhang, W.; Tian, H.; Han, L.; Zhu, W.-H., Efficient and Stable Chemical Passivation on Perovskite Surface via Bidentate Anchoring. *Advanced Energy Materials* **2019,** *9* (13), 1803573.
45. Noel, N. K.; Abate, A.; Stranks, S. D.; Parrott, E. S.; Burlakov, V. M.; Goriely, A.; Snaith, H. J., Enhanced Photoluminescence and Solar Cell Performance via Lewis Base Passivation of Organic–Inorganic Lead Halide Perovskites. *ACS Nano* **2014,** *8* (10), 9815-9821.
46. Yang, S.; Dai, J.; Yu, Z.; Shao, Y.; Zhou, Y.; Xiao, X.; Zeng, X. C.; Huang, J., Tailoring Passivation Molecular Structures for Extremely Small Open-Circuit Voltage Loss in Perovskite Solar Cells. *Journal of the American Chemical Society* **2019,** *141* (14), 5781-5787.
47. Wang, Q.; Mosconi, E.; Wolff, C.; Li, J.; Neher, D.; De Angelis, F.; Suranna, G. P.; Grisorio, R.; Abate, A., Rationalizing the Molecular Design of Hole-Selective Contacts to Improve Charge Extraction in Perovskite Solar Cells. *Advanced Energy Materials* **2019,** *9* (28), 1900990.
48. Quarti, C.; De Angelis, F.; Beljonne, D., Influence of Surface Termination on the Energy Level Alignment at the CH3NH3PbI3 Perovskite/C60 Interface. *Chemistry of Materials* **2017,** *29* (3), 958-968.
49. Meggiolaro, D.; Mosconi, E.; Proppe, A. H.; Quintero-Bermudez, R.; Kelley, S. O.; Sargent, E. H.; De Angelis, F., Energy Level Tuning at the MAPbI3 Perovskite/Contact Interface Using Chemical Treatment. *ACS Energy Letters* **2019,** *4* (9), 2181-2184.
50. Perdew, J. P.; Ernzerhof, M.; Burke, K., Rationale for mixing exact exchange with density functional approximations. *The Journal of chemical physics* **1996,** *105* (22), 9982-9985.
51. Adamo, C.; Barone, V., Toward reliable density functional methods without adjustable parameters: The PBE0 model. *The Journal of chemical physics* **1999,** *110* (13), 6158-6170.
52. Perdew, J. P.; Parr, R. G.; Levy, M.; Balduz, J. L., Density-Functional Theory for Fractional Particle Number: Derivative Discontinuities of the Energy. *Physical Review Letters* **1982,** *49* (23), 1691-1694.
53. Miceli, G.; Chen, W.; Reshetnyak, I.; Pasquarello, A., Nonempirical hybrid functionals for band gaps and polaronic distortions in solids. *Physical Review B* **2018,** *97* (12), 121112.

54. Nguyen, N. L.; Colonna, N.; Ferretti, A.; Marzari, N., Koopmans-Compliant Spectral Functionals for Extended Systems. *Physical Review X* **2018,** *8* (2), 021051.
55. Vydrov, O. A.; Van Voorhis, T., Nonlocal van der Waals density functional: The simpler the better. *The Journal of chemical physics* **2010,** *133* (24), 244103.
56. Sabatini, R.; Gorni, T.; De Gironcoli, S., Nonlocal van der Waals density functional made simple and efficient. *Physical Review B* **2013,** *87* (4), 041108.
57. VandeVondele, J.; Krack, M.; Mohamed, F.; Parrinello, M.; Chassaing, T.; Hutter, J., Quickstep: Fast and accurate density functional calculations using a mixed Gaussian and plane waves approach. *Computer Physics Communications* **2005,** *167* (2), 103-128.
58. Goedecker, S.; Teter, M.; Hutter, J., Separable dual-space Gaussian pseudopotentials. *Physical Review B* **1996,** *54* (3), 1703.
59. VandeVondele, J.; Hutter, J., Gaussian basis sets for accurate calculations on molecular systems in gas and condensed phases. *The Journal of Chemical Physics* **2007,** *127* (11), 114105.
60. Guidon, M.; Hutter, J.; VandeVondele, J., Auxiliary Density Matrix Methods for Hartree−Fock Exchange Calculations. *Journal of Chemical Theory and Computation* **2010,** *6* (8), 2348-2364.
61. Even, J.; Pedesseau, L.; Jancu, J.-M.; Katan, C., Importance of Spin–Orbit Coupling in Hybrid Organic/Inorganic Perovskites for Photovoltaic Applications. *The Journal of Physical Chemistry Letters* **2013,** *4* (17), 2999-3005.
62. Umari, P.; Mosconi, E.; De Angelis, F., Relativistic GW calculations on CH3NH3PbI3 and CH3NH3SnI3 Perovskites for Solar Cell Applications. *Scientific Reports* **2014,** *4*, 4467.
63. Meggiolaro, D.; De Angelis, F., First-Principles Modeling of Defects in Lead Halide Perovskites: Best Practices and Open Issues. *ACS Energy Letters* **2018,** *3* (9), 2206-2222.
64. Mahata, A.; Meggiolaro, D.; De Angelis, F., From Large to Small Polarons in Lead, Tin, and Mixed Lead–Tin Halide Perovskites. *The Journal of Physical Chemistry Letters* **2019,** *10* (8), 1790-1798.
65. Meggiolaro, D.; Ambrosio, F.; Mosconi, E.; Mahata, A.; De Angelis, F., Polarons in Metal Halide Perovskites. *Advanced Energy Materials* **2019,** *n/a* (n/a), 1902748.
66. Haruyama, J.; Sodeyama, K.; Han, L.; Tateyama, Y., Surface Properties of CH3NH3PbI3 for Perovskite Solar Cells. *Accounts of Chemical Research* **2016,** *49* (3), 554-561.
67. Baikie, T.; Fang, Y.; Kadro, J. M.; Schreyer, M.; Wei, F.; Mhaisalkar, S. G.; Graetzel, M.; White, T. J., Synthesis and crystal chemistry of the hybrid perovskite (CH3NH3)PbI3 for solid-state sensitised solar cell applications. *Journal of Materials Chemistry A* **2013,** *1* (18), 5628-5641.
68. Komsa, H.-P.; Rantala, T. T.; Pasquarello, A., Finite-size supercell correction schemes for charged defect calculations. *Physical Review B* **2012,** *86* (4), 045112.
69. Freysoldt, C.; Grabowski, B.; Hickel, T.; Neugebauer, J.; Kresse, G.; Janotti, A.; Van de Walle, C. G., First-principles calculations for point defects in solids. *Reviews of Modern Physics* **2014,** *86* (1), 253-305.
70. Freysoldt, C.; Neugebauer, J.; Van de Walle, C. G., Fully Ab Initio Finite-Size Corrections for Charged-Defect Supercell Calculations. *Physical Review Letters* **2009,** *102* (1), 016402.
71. Komsa, H.-P.; Pasquarello, A., Finite-Size Supercell Correction for Charged Defects at Surfaces and Interfaces. *Physical Review Letters* **2013,** *110* (9), 095505.
72. Halgren, T. A.; Lipscomb, W. N., The synchronous-transit method for determining reaction pathways and locating molecular transition states. *Chemical Physics Letters* **1977,** *49* (2), 225-232.
73. Zheng, K.; Abdellah, M.; Zhu, Q.; Kong, Q.; Jennings, G.; Kurtz, C. A.; Messing, M. E.; Niu, Y.; Gosztola, D. J.; Al-Marri, M. J.; Zhang, X.; Pullerits, T.; Canton, S. E., Direct Experimental Evidence for Photoinduced Strong-Coupling Polarons in Organolead Halide Perovskite Nanoparticles. *The Journal of Physical Chemistry Letters* **2016,** *7* (22), 4535-4539.
74. Sadoughi, G.; Starr, D. E.; Handick, E.; Stranks, S. D.; Gorgoi, M.; Wilks, R. G.; Bär, M.; Snaith, H. J., Observation and Mediation of the Presence of Metallic Lead in Organic–Inorganic Perovskite Films. *ACS Applied Materials & Interfaces* **2015,** *7* (24), 13440-13444.
75. Giannozzi, P.; Baroni, S.; Bonini, N.; Calandra, M.; Car, R.; Cavazzoni, C.; Ceresoli, D.; Chiarotti, G. L.; Cococcioni, M.; Dabo, I.; Dal Corso, A.; de Gironcoli, S.; Fabris, S.; Fratesi, G.; Gebauer, R.; Gerstmann, U.; Gougoussis, C.; Kokalj, A.; Lazzeri, M.; Martin-Samos, L.; Marzari, N.; Mauri, F.; Mazzarello, R.; Paolini, S.; Pasquarello, A.; Paulatto, L.; Sbraccia, C.; Scandolo, S.; Sclauzero, G.; Seitsonen, A. P.; Smogunov, A.; Umari, P.; Wentzcovitch, R. M., QUANTUM ESPRESSO: a modular and

open-source software project for quantum simulations of materials. *Journal of Physics: Condensed Matter* **2009,** *21* (39), 395502.
76. Hamann, D. R., Optimized norm-conserving Vanderbilt pseudopotentials. *Physical Review B* **2013,** *88* (8), 085117.
77. Perdew, J. P.; Burke, K.; Ernzerhof, M., Generalized Gradient Approximation Made Simple. *Physical Review Letters* **1996,** *77* (18), 3865-3868.
78. Zhu, H.; Trinh, M. T.; Wang, J.; Fu, Y.; Joshi, P. P.; Miyata, K.; Jin, S.; Zhu, X. Y., Organic Cations Might Not Be Essential to the Remarkable Properties of Band Edge Carriers in Lead Halide Perovskites. *Advanced Materials* **2017,** *29* (1), 1603072.
79. Evans, T. J. S.; Miyata, K.; Joshi, P. P.; Maehrlein, S.; Liu, F.; Zhu, X. Y., Competition Between Hot-Electron Cooling and Large Polaron Screening in CsPbBr3 Perovskite Single Crystals. *The Journal of Physical Chemistry C* **2018,** *122* (25), 13724-13730.
80. Zhu, X. Y.; Podzorov, V., Charge Carriers in Hybrid Organic–Inorganic Lead Halide Perovskites Might Be Protected as Large Polarons. *The Journal of Physical Chemistry Letters* **2015,** *6* (23), 4758-4761.
81. Diab, H.; Trippé-Allard, G.; Lédée, F.; Jemli, K.; Vilar, C.; Bouchez, G.; Jacques, V. L. R.; Tejeda, A.; Even, J.; Lauret, J.-S.; Deleporte, E.; Garrot, D., Narrow Linewidth Excitonic Emission in Organic–Inorganic Lead Iodide Perovskite Single Crystals. *The Journal of Physical Chemistry Letters* **2016,** *7* (24), 5093-5100.
82. Meggiolaro, D.; Motti, S. G.; Mosconi, E.; Barker, A. J.; Ball, J.; Andrea Riccardo Perini, C.; Deschler, F.; Petrozza, A.; De Angelis, F., Iodine chemistry determines the defect tolerance of lead-halide perovskites. *Energy & Environmental Science* **2018,** *11* (3), 702-713.
83. Yamada, Y.; Nakamura, T.; Endo, M.; Wakamiya, A.; Kanemitsu, Y., Near-band-edge optical responses of solution-processed organic–inorganic hybrid perovskite CH3NH3PbI3on mesoporous TiO2electrodes. *Applied Physics Express* **2014,** *7* (3), 032302.
84. Yin, W.-J.; Shi, T.; Yan, Y., Unusual defect physics in CH3NH3PbI3 perovskite solar cell absorber. *Applied Physics Letters* **2014,** *104* (6), 063903.
85. Kang, J.; Wang, L.-W., High Defect Tolerance in Lead Halide Perovskite CsPbBr3. *The Journal of Physical Chemistry Letters* **2017,** *8* (2), 489-493.